IEEE Access
Multidisciplinary | Rapid Review | Open Access Journal

Received November 22, 2020, accepted December 24, 2020, date of publication January 1, 2021, date of current version February 5, 2021.

Digital Object Identifier 10.1109/ACCESS.2020.3048712

Decomposed Mean Euler-Poincaré Characteristic Model for a Non-Gaussian Physiological Random Field

MOISES RAMOS-MARTINEZ[1], CHRISTOPHE CORBIER[2], VICTOR M. ALVARADO[1], AND GUADALUPE LOPEZ LOPEZ[1]

[1]TecNM/CENIDET, Int. Internado Palmira s/n, 62490 Cuernavaca, Mexico
[2]LASPI, IUT de Roanne, Université de Saint-Etienne, 42334 Saint-Etienne, France

Corresponding author: Victor M. Alvarado (victor@alvarado.fr)

ABSTRACT This paper introduces a new approach of the mean Euler-Poincaré characteristic for non-Gaussian random fields (NGRF), which is based on the decomposition by a basic function named *mother-wave*. The method is proved for long-term recorded, noisy physiological signals. A pretreatment allows the signal to become smooth as the original one is fitted through a Random Algebraic Polynomials (RAP)-based scheme. After that, the polynomized signals are merged by thresholding the RAP function at different levels u. In this way, it is formed a real-valued non-Gaussian physiological random field (NGPRF). Thereby, we deal with their geometric properties centered on their excursion sets $A_u(\Phi, \mathcal{T})$ and a topological invariant, such as the Euler Poincaré Characteristic (EPC) $\varphi(A_u(\Phi, \mathcal{T}))$. The highlight of this work is an explicit model, referred to as the decomposed mean Euler-Poincaré characteristic (DMEPC). The proposed method produces a reduced model with a viable interpretation for different heart conditions investigated for data issued from Holter EKG recordings.

INDEX TERMS DMEPC, Euler characteristic, random field.

I. INTRODUCTION

Random Fields (RF) give a statistical description of complex random patterns of change and relationships from physical data sets [1]–[3]. Consider a random variable $\Phi(\boldsymbol{X}, \bullet)$ as a function of $\boldsymbol{X} = [X_1, \ldots, X_n]^T$ with $\{X_k\}_{k=1}^n$ as the set of random continuous coordinates, then, a collection of $\Phi(\boldsymbol{X}, \bullet)$ is named random field [4]. The geometry and regularity properties of RF have been largely discussed in the literature. These features have to do with continuity and differentiability notions [5] and still with the geometry generated by RF through their excursion sets over a level u [4]. Gaussian Random Fields (GRF) is a class of RF for which the finite-dimensional distributions are multivariable normal distributions that can be fully specified by expectations and covariances. GRFs lead to a large class of applications suited for use in mathematics, sciences, and engineering [6]. A noticeable issue has been accessing information from biomedical images. In this case, Gaussian Markov Random Fields (GMRF) provide a spatial-contextual knowledge that has often resulted in spatial statistics applications. The research by [7] used Markov irregular fields (MRF) to address biomedical image analysis by image segmentation, object labeling, and 3D vision. Later, [8] developed a Bayesian framework that introduces an adjustable parameter on a Generalized Adaptive Gaussian Markov random field (GAGMRF) model to adjust the image quality for X-ray Luminescence tomographies. Researches that engage in RF concern also medical analyses. As an example, we refer to the work in [9], where statistical methods assisted morphometric analyses of specific subregions of the brain. Here, using GRF differentiated the shape of the amygdala and the hippocampus of normal subjects face to patients with attention-deficit/hyperactivity disorder (ADHD). Another type of RF usage points to disease mapping. In this regard, we cite the work of [10] that propose a Bayesian analysis of a GMRF to determine the spatial variability of lip cancer cases in Scotland for a period of five years.

From the given literature review, we deduce that the theory of GRF supports quite well medical diagnosis practice by images. However, for some diseases, the diagnosis is made more by reading signals recorded over time. For example,

The associate editor coordinating the review of this manuscript and approving it for publication was Aniruddha Datta.

an electrocardiogram (EKG) is a standard description of the heart's electrical signals. The interpretation of the EKG data helps to distinguish heart disorders. The visual inspection of an EKG can be bulky and can lead to misinterpretation. As a result, computer-assisted algorithms have emerged to handle EKG data with the aim of improving the detection of heart conditions.

Opposite to the computer-aided diagnosis by biological images, which add RF advancements, to our knowledge, there is not automated diagnosis by physiological signals based on the theory of RF. Instead, signal processing is made by transforming the temporal data to the frequency domain. In this transformation, statistical features are obtained. Then, the gained knowledge is the input of a classifier. The classification rules serve to distinguish distinct cardiac conditions. It is worthy of keeping in mind that the full treatment is applied beat by beat, hence with a high computational burden.

Otherwise, this work aims to provide a method to handle extensive noisy physiological data. The central idea is to extract a geometrical structure to build a non-Gaussian Random Field (NGRF). The paper's highlight is the formulation of an explicit mathematical model of the built NGRF. To fix the mathematical basis, we use the main elements of the GRF theory. A complete methodology to exploit this approach is not within the scope of this paper. However, we explore the effectiveness of our approach by decomposing Holter monitor signals. The Holter test monitors an ambulatory patient during long periods (24 to 48 h). The NGRF built from the Holter tests separates the P and T pics of the EKG of the entire test. The outcome is a reduced description of the heart's electrical signals. The assumption is that some patterns can be identified that can help in giving medical prevention insights. In this way, the foundations are laid for further development.

[1], along with extensions of Worsley [11]–[13], combined the geometry of topology with probability and statistics. The resulting theory has become a standard framework to analyzing RF. Central concepts of this theory are the excursion set $A_u(\Phi, \mathcal{T})$ with $\mathcal{T}$ a topological space, and the Euler-Poincaré characteristic (EPC) $\varphi(A_u(\Phi, \mathcal{T}))$. The excursion set is simply the set of points where the RF exceeds a fixed threshold value $u \in \mathbb{R}$, whereas the EPC lets us know about the topology of this set. The EPC is a topological invariant that counts the number of connected components in the excursion set minus the number of holes [14]. Among other purposes, a descriptor based on EPC was presented in [14] to classify images and 3D mesh surfaces.

Summing up, [1] estimated the geometric structure of the excursion sets for real-valued Gaussian RF by differential topology (DT) and integral geometry (IG). This approach delivers the theory and conditions for a smooth GRF with a smooth boundary $\partial\mathcal{T}$. With this scheme, the average data subtracted from numerous trials are standardized by the mean Euler-Poincaré characteristic (MEPC), which is denoted by $\mathbb{E}\{\varphi(A_u(\Phi, \mathcal{T}))\}$. Adler (1981) defined the DT (differential topology) characteristic of the excursion set so that it meets the EPC when the excursion set does not touch the boundary. Then, a limit correction providing the MEPC itself in $\mathbb{R}^2$ and $\mathbb{R}^3$ was found by Worsley [15]. A significant outcome of the RF theory has been an explicit formula of the expected MEPC for smooth RF. In order to get this kind of RF, in our approach, the physiological data fit random algebraic polynomials (RAP). The suggested polynomization procedure is comparable to digital filtering techniques.

RAP are relevant to engineering, physics or economics goals. A notable work written by Bharucha and Sambandham [16] examined and described the properties of random orthogonal and trigonometric polynomials. A deal for using RAP is to identify the number of real zeros. In this regard, Kac [17] gave the formula to get the expected number of real zeros of a RAP. Among the studies that implement the Kac's formula we found, for example, [18], [19], and [20]. Likewise, some methods are encountered that find the real zeros of RAP, e.g. a quadratically convergent iterative procedure to find all zeros simultaneously is given [21], [22], with a basis on the Gerschgorin's theorems [23].

The theory of Adler and Taylor has been extended to Gaussian-related RF (namely, χ^2, $\mathcal{F}$, and t fields) [15]. Later, [4] further study the excursion sets of non-Gaussian random fields (NGRF) holding high levels. High peaks in an RF are due to noise, high frequencies, states, or other behaviors. Besides, the high levels in RF lead to complicated geometry and render NGRF features. In [1], pages 387-433, it was presented a special description of NGRF of the form $f(t) = F(y(t)) = F(y_1(t), \ldots, y_k(t))$ where the $y_j(t)$ are a collection of independent, identically distributed (i.i.d.) GRF. Because limited cases can be defined in this way, and it is difficult to get a function F to encode the behavior of NGRF, we introduce an approach focused on the MEPC. We propose a new characteristic through a decomposition that we refer to as the decomposed mean Euler-Poincaré characteristic (DMEPC).

We are interested in the geometric properties of real-valued Non-Gaussian RF with a focus on their excursion sets $A_u(\Phi, \mathcal{T})$. An outcome of this work is an explicit model of a decomposed expected Euler characteristic $\mathbb{E}\{\varphi(A_u(\Phi, \mathcal{T}))\}$ of the excursion set of an NGRF. The implementation of our approach relies on data from electrocardiograph (EKG) signals whereby an NGRF is built.

From a medical point of view, a recognized method to diagnose cardiovascular diseases is to analyze EKG signals. We chose to work with Holter EKG data from the SHAREE database [24]. The objective is to model the Holter EKG behavior. Our methodology is as follows. First, we fit the Holter data with RAP to get a smoothed signal. Then, we transform the polynomized cycles into an RF. These signals are collapsed to build a smooth NGRF with high peaks by thresholding the RAP function at different levels u. Lastly, we propose a decomposed MEPC linked to the built NGRF. It is a quite reduced version of the original Holter EKG signal, intended to be read easier. Some patterns are acknowledged for certain heart conditions.

The manuscript is organized as follows: In Section II, we introduce the mathematical aspects and model for the

DMPEC method. In Section III, experimental results are discussed to classify MI from Holter EKG signals. Finally, we provide a conclusion in Section IV. Proofs of Theorems and Lemmas are provided in Appendices.

II. MATHEMATICAL FRAMEWORK

A. POLYNOMIZATION

Polynomization is a modeling based on RAP denoted $\psi(\bullet, X_1)$ of a EKG cycle c ($c = 1 \dots N$) where, for a fixed threshold, each of them can be decomposed over two intervals $I_1(c) = \begin{bmatrix}1 & X^R(c)\end{bmatrix}$ and $I_2(c) = \begin{bmatrix}X^R(c) & X^E(c)\end{bmatrix}$ with $X^R(c)$ index-time of the R wave. Let $\{a_k(c, \overline{\omega})\}_{k=1}^{D(c)}$ be a sequence of i.i.d. random variables and $\psi_B(\mathcal{E}, \overline{\omega}, X_1(c))$ be a basic RAP of order $D(c)$ defined by

$$\psi_B(\mathcal{E}, \overline{\omega}, X_1(c)) = \sum\nolimits_{k=0}^{D(c)} a_k(c, \overline{\omega}) X_1(c)^k, \tag{1}$$

with $\mathcal{E} = \left(\overline{\Omega}, \overline{\Sigma}, P\right)$ a complete probability space where $\overline{\Omega}$ denotes the sample space, $\overline{\Sigma}$ a σ-algebra on $\overline{\Omega}$ and P a probability measure on $\overline{\Sigma}$. For each interval $I_m(c)$ ($m = 1, 2$) define a RAP as $\psi_D^m(\mathcal{E}, \overline{\omega}, X_1(c)) = \psi_B(\mathcal{E}, \overline{\omega}, X_1(c)) \mathbf{1}_{I_m(c)}$ where $\mathbf{1}_X$ is the unit function over X. The polynomization over one cycle c can then be written as

$$\psi_D(\mathcal{E}, \overline{\omega}, X_1(c)) = \sum\nolimits_{k=0}^{D_1(c)} a_k^{I_1}(c, \overline{\omega}) (X_1^{I_1}(c))^k + \sum\nolimits_{k=0}^{D_2(c)} a_k^{I_2}(c, \overline{\omega}) (X_1^{I_2}(c))^k. \tag{2}$$

B. MODELING NON-GAUSSIAN RANDOM FIELD

Let $\Phi(\boldsymbol{X}, \overline{\omega})$ be a NGRF at $\boldsymbol{X}$ with $\boldsymbol{X} = [X_1(c) \;\; X_2]^T$ where $X_1(c) \in I_1(c) \cup I_2(c)$. Let $\mathcal{E} = \left(\overline{\Omega}, \overline{\Sigma}, P\right)$ be a complete probability space and $\mathcal{T}$ a topological space, where $\overline{\Omega}$ denotes the sample space, $\overline{\Sigma}$ a σ-algebra on $\overline{\Omega}$ and P a probability measure on $\overline{\Sigma}$. Then a measurable mapping $\Phi : \overline{\Omega} \to \mathbb{R}^{\mathcal{T}}$ is called a real-valued random field. Here $\boldsymbol{X} \in \mathcal{T} \subset \mathbb{R}^2$ and Φ is called an 2-dimensional NGRF over N cycles defined as

$$\Phi(X_1, X_2, \overline{\omega}) = \Phi(\boldsymbol{X}, \overline{\omega}) = \sum_{c=1}^{N} \psi_D(\mathcal{E}, \overline{\omega}, X_1(c)) \delta(c - X_2), \tag{3}$$

where δ is the Dirac's distribution. Eq.(3) means that each EKG signal for a fixed threshold is decomposed into basic RAP $\psi_D(\mathcal{E}, \overline{\omega}, X_1(c))$ to form a NGRF according to the coordinate X_2.

C. NON-GAUSSIAN RANDOM FIELD

The most important concept in the random field theory is named *excursion set*. Let $\Phi(\boldsymbol{X}, \overline{\omega})$ be a NGRF, $\boldsymbol{X} \in \mathcal{T} \subset \mathbb{R}^2$, defined inside a set $\mathcal{T}$. The excursion set is a geometrical object defined as

$$\mathcal{A}_u(\Phi, \mathcal{T}) = \{\boldsymbol{X} \in \mathcal{T}, \Phi(\boldsymbol{X}, \overline{\omega}) \geq u\}. \tag{4}$$

Thus $\mathcal{A}_u$ of $\Phi(\boldsymbol{X}, \overline{\omega})$ above a threshold u is the set of points in $\mathcal{T} \subset \mathbb{R}^2$ where $\Phi(\boldsymbol{X}, \overline{\omega})$ exceeds u. Remember that stratified manifolds $\mathcal{T}$ in $\mathbb{R}^2$ are basically sets that can be partitioned into the disjoint union of manifolds as $\mathcal{T} = \cup_{j=0}^{dim\mathcal{T}} \partial_j \mathcal{T}$ where each stratum $\partial_j \mathcal{T}$ is itself a disjoint union of a number of j-dimensional manifolds. Here non-Gaussian properties of Φ involve to consider a class of generalization of random fields of the form

$$\Phi(\boldsymbol{X}, \overline{\omega}) = F(\phi_*(\boldsymbol{X}, \overline{\omega})) = F\left(\phi_*^1(\boldsymbol{X}, \overline{\omega}), \dots, \phi_*^m(\boldsymbol{X}, \overline{\omega})\right), \tag{5}$$

are defined, where $\phi_*^j(\boldsymbol{X}, \overline{\omega})$ are a collection of i.i.d. Gaussian random fields (GRF), all defined over a topological space $\mathcal{T}$ and $F : \mathbb{R}^m \to \mathbb{R}$ is a smooth function to be picewise C^2, along with appropriate side conditions. The excursion set of a real-valued non-Gaussian $\Phi = F \circ \phi_*$ above a level u is equivalent to the excursion set for a vector-valued Gaussian ϕ_* in $F^{-1}[u, \infty)$ and given by

$$\mathcal{A}_u(\Phi, \mathcal{T}) = \mathcal{A}_u(F \circ \phi_*, \mathcal{T}) = \{\boldsymbol{X} \in \mathcal{T}, (F \circ \phi_*)(\boldsymbol{X}, \overline{\omega}) \geq u\}. \tag{6}$$

In our framework let $\Sigma_s = (s_1, \dots s_{S^M})$ be the set of *signatures* with s_k the associated signed unit weight (SUW) for each sub GRF $\phi^{s_k}(\boldsymbol{X}, \overline{\omega})$ and $S^M = \sum_{k=1}^{M} (-1)^k s_k$. Let us define the NGRF given by Eq.(3) as

$$\Phi(\boldsymbol{X}, \overline{\omega}, S^M) = \left(s_1 \phi^{s_1}(\boldsymbol{X}, \overline{\omega}), \dots, s_{S^M} \phi^{s_{S^M}}(\boldsymbol{X}, \overline{\omega})\right), \tag{7}$$

where $s_m \phi^{s_m}(\boldsymbol{X}, \overline{\omega})$ ($m = 1 \dots S^M$) is a collection of i.i.d. *signed* GRF with $\boldsymbol{X} \in \mathbb{R}^2$, $\overline{\omega} \in \overline{\Omega}$ and $s_{2n} = +1$, $s_{2n+1} = -1$.

D. MEAN EULER-POINCARÉ CHARACTERISTIC

Now denote the EPC of a set $\mathcal{A}_u(\Phi, \mathcal{T})$ by $\varphi(\mathcal{A}_u(\Phi, \mathcal{T}))$. For numerous trials, consider that $\mathbb{E}\{\varphi(\mathcal{A}_u(\Phi, \mathcal{T}))\}$ is computable. Therefore the random fields theory impose some regularity conditions on $\Phi(\boldsymbol{X}, \overline{\omega})$ to ensure both, that its realisations are smooth and the boundary $\partial\mathcal{T}$ is smooth. Then $\mathcal{T}$ is a regular C^2 domain in a compact t subset of $\mathbb{R}^2$ bounded by a regular 1-dimensional manifold $\partial\mathcal{T}$ of classe C^2. Consider $\Phi(\boldsymbol{X}, \overline{\omega})$, $\boldsymbol{X} = [X_1, X_2] \in \mathbb{R}^2$ a stationary non isotropic random field and $\dot{\Phi}_j(\boldsymbol{X}, \overline{\omega}) = \dfrac{\partial \Phi(\boldsymbol{X}, \overline{\omega})}{\partial X_j}$, $\ddot{\Phi}_{jk}(\boldsymbol{X}, \overline{\omega}) = \dfrac{\partial^2 \Phi(\boldsymbol{X}, \overline{\omega})}{\partial X_j \partial X_k}$, $j, k = 1, 2$. The moduli of continuity of $\dot{\Phi}_j(\boldsymbol{X}, \overline{\omega})$ and $\ddot{\Phi}_{jk}(\boldsymbol{X}, \overline{\omega})$ inside $\mathcal{T}$ are given by $\omega_j(h) = \sup_{\|\boldsymbol{X}-\boldsymbol{Y}\|<h, \overline{\omega}} |\dot{\Phi}_j(\boldsymbol{X}, \overline{\omega}) - \dot{\Phi}_j(\boldsymbol{Y}, \overline{\omega})|$ and $\omega_{jk}(h) = \sup_{\|\boldsymbol{X}-\boldsymbol{Y}\|<h, \overline{\omega}} |\ddot{\Phi}_{jk}(\boldsymbol{X}, \overline{\omega}) - \ddot{\Phi}_{jk}(\boldsymbol{Y}, \overline{\omega})|$, respectively. To ensure that realisations of $\Phi(\boldsymbol{X}, \overline{\omega})$ are sufficiently smooth, consider the following conditions

- C1: $\mathbb{P}\left(\max_{j,k}\left\{\omega_j(h), \omega_{jk}(h)\right\} > \epsilon\right) = o(h^N)$ as $h \downarrow 0$,
- C2: Hessian matrix $\ddot{\boldsymbol{\Phi}}$ of $\ddot{\Phi}_{jk}$ has finite variance conditional on $\left(\Phi, \dot{\boldsymbol{\Phi}}\right)$ with $\dot{\boldsymbol{\Phi}}$ grandient of $\dot{\Phi}_j$,
- C3: the density of $\left(\Phi, \dot{\boldsymbol{\Phi}}\right)$ is bounded above, uniformly for all $\boldsymbol{X} \in \mathcal{T}$.

At a point $\boldsymbol{X} \in \partial\mathcal{T}$, let $\dot{\Phi}_\perp$ be the gradient of Φ in the direction of the inside normal to $\partial\mathcal{T}$, let $\dot{\boldsymbol{\Phi}}_T$ be the gradient 1-vector in the tangent plane to $\partial\mathcal{T}$, let $\ddot{\boldsymbol{\Phi}}_T$ be the

1×1-Hessian matrix in the tangent plane to $\partial\mathcal{T}$ and let $\boldsymbol{r}$ be the 1×1 inside curvature matrix of $\partial\mathcal{T}$. Let *sign* be the sign function. Consider the notation of Knuth [25] where a logical expression in parentheses takes the value one if true and zero otherwise. Under conditions C1-C3, then the EPC is

$$\begin{aligned}\varphi(\mathcal{A}_u(\Phi,\mathcal{T})) = &\sum\nolimits_{\boldsymbol{X}\in\mathcal{T}} (\Phi \geq u)\left(\dot{\boldsymbol{\Phi}} = \boldsymbol{0}\right) sign\left[det(-\ddot{\boldsymbol{\Phi}})\right] \\ &+ \sum\nolimits_{\boldsymbol{X}\in\partial\mathcal{T}} (\Phi \geq u)\left(\dot{\boldsymbol{\Phi}}_T = \boldsymbol{0}\right)\left(\dot{\Phi}_\perp < 0\right) \\ &\times sign\left[det(-\ddot{\boldsymbol{\Phi}}_T - \dot{\Phi}_\perp \boldsymbol{r})\right], \end{aligned} \tag{8}$$

with probability one. In $\mathbb{R}^2$ integral geometry defines $\varphi(\mathcal{A}_u(\Phi,\mathcal{T}))$ as (the number of connected components)-(the number of holes) in $\mathcal{A}_u(\Phi,\mathcal{T})$. Moreover remember that the expectation of $\varphi(\mathcal{A}_u(\Phi,\mathcal{T}))$ for multiple realisations is

$$\begin{aligned}&\mathbb{E}\left\{\varphi(\mathcal{A}_u(\Phi,\mathcal{T}))\right\} \\ &= \int_{\mathcal{T}} \mathbb{E}\left\{(\Phi \geq u)\, det(-\ddot{\boldsymbol{\Phi}}) \mid \dot{\boldsymbol{\Phi}} = \boldsymbol{0}\right\}\theta(\boldsymbol{0})d\boldsymbol{X} \\ &\quad + \int_{\partial\mathcal{T}} \mathbb{E}\left\{(\Phi \geq u)\,(\dot{\Phi}_\perp < 0)\, det\left(-\ddot{\boldsymbol{\Phi}}_T - \dot{\Phi}_\perp \boldsymbol{r}\right) \mid \dot{\boldsymbol{\Phi}}_T = \boldsymbol{0}\right\} \\ &\quad \times \theta_T(\boldsymbol{0})d\boldsymbol{X}, \end{aligned} \tag{9}$$

where $\theta(.)$ is the density of $\dot{\Phi}$ and $\theta_T(.)$ is the density of $\dot{\Phi}_T$. Worsley in [26] showed that under the slightly more general condition where the boundary of $\mathcal{T}$ is composed of a finite number of piecewise smooth components, then the expectation of the excursion sets of a random field with zero mean and unit variance is

$$\mathbb{E}\left\{\varphi(\mathcal{A}_u(\Phi,\mathcal{T}))\right\} = \sum\nolimits_{j=0}^{N} \rho_j(u)\mathcal{L}_j(\mathcal{T}) \tag{10}$$

where $\rho_j(u) = (2\pi)^{-(j+1)/2} H_{j-1}(u)\exp(-u^2/2)$ is the *intensity* of the EPC per unit volume, H_j the *jth* Hermite polynomial and $\mathcal{L}_j(\mathcal{T})$ the Lipschitz-Killing curvatures.

E. VOLUME OF TUBES

Volume of tubes approach for a class of Gaussian processes is linked to a finite Karhunen-Loéve expansion. These are processes defined on a manifold $\mathcal{T}$ that can be expressed as

$$\phi(\boldsymbol{X},\overline{\omega}) = \langle\alpha(\boldsymbol{X}), \xi(\overline{\omega})\rangle_{\mathbb{R}^l} = \sum\nolimits_{j=1}^{l} \alpha_j(\boldsymbol{X})\xi_j(\overline{\omega}) \tag{11}$$

for some smooth mapping $\alpha : \mathcal{T} \longrightarrow S(\mathbb{R}^l)$ where ξ_j are independent standard Gaussians and $S(\mathbb{R}^l)$ the sphere in $\mathbb{R}^l$, $l \geq 1$. Consider a metric space $(\mathcal{T},\tau)$ as $S(\mathbb{R}^l)$ with a geodesic metric $\tau(x,y) = cos^{-1}(\langle x,y\rangle)$. Then a tube of radius ρ around a closed set A is $Tube(A,\rho) = \left\{x \in S(\mathbb{R}^l) : \sup_{y\in A}\langle x,y\rangle \geq cos(\rho)\right\}$. In the case where X is a random vector uniformly distributed on $S(\mathbb{R}^l)$ with distribution η_l then

$$\mathbb{P}\left\{\sup_{y\in A}\langle X,y\rangle \geq cos(\rho)\right\} = \eta_l\left(Tube(A,\rho)\right).$$

Consider $\mathcal{H}_N$ the N-dimensional Hausdorff measure associated with the geodesic metric τ. Remember the Weyl's tube formula on $S(\mathbb{R}^l)$. Assume $\mathcal{T}$ is a C^2, locally convex, Whitney stratified submanifold of $S_\lambda(\mathbb{R}^l)$, the sphere of radius λ. For $\rho < \rho_c\left(\mathcal{T}, S_\lambda(\mathbb{R}^l)\right)$

$$\begin{aligned}&\mathcal{H}_{l-1}\left(Tube(\mathcal{T},\rho)\right) \\ &= \sum_{j=0}^{N}\left(\sum_{n=0}^{\lfloor\frac{j}{2}\rfloor}\frac{(-4\pi)^{-n}\lambda^{l-1+j}j!G_{j-2n,l-1+2n-j}(\frac{\rho}{\lambda})}{n!(j-2n)!}\right)\mathcal{L}_j(\mathcal{T}),\end{aligned} \tag{12}$$

where $G_{a,b}(\rho) = \dfrac{\pi^{b/2}}{b\Gamma(b/2+1)}\int_0^\rho cos^a(r)sin^{b-1}(r)dr$, $\lfloor n\rfloor$ is the integer less than n and $\mathcal{L}_j(\mathcal{T})$ the Lipschitz-Killing curvatures (LKC) given for a measurable subsets U by

$$\mathcal{L}_j(\mathcal{T}) = \frac{(-2\pi)^{-(N-j)/2}}{((N-j)/2)!}\int_U Tr^{\mathcal{T}}(R^{(N-j)/2})Vol_g$$

if $N-j$ is even and 0 otherwise. Tr is the trace, R is the Riemannian curvature tensor and Vol_g is the Riemannian volume form on the metric tensor g. Remark that LKC is the EPC for $j=0$, the perimeter of $\partial\mathcal{T}$ for $j=1$ and the area of $\mathcal{T}$ for $j=2$.

F. DECOMPOSED MEAN EULER-POINCARÉ CHARACTERISTIC

Now we present our approach related to a new modeling of MEPC based decomposition. In our context of sub signed GRF $\phi^{s_k}(\boldsymbol{X},\overline{\omega})$ to form the NGRF $\Phi(\boldsymbol{X},\overline{\omega},S^M)$ the volume of tubes is required to prove our following Lemma.

Lemma 1: Let $\mathcal{T}$ be a C^2 manifold in $\mathbb{R}^N$ $(N \geq 1)$, locally convex, Whitney stratified submanifold of $S_1(\mathbb{R}^l)$. Let $s_k\alpha^{s_k}(\boldsymbol{X}), k = 1,\ldots,S^M$ be deterministic coefficients for $s_k \in \Sigma_s$ *and* $\xi(\overline{\omega})$ be independent standard Gaussians. Let $s_k\phi^{s_k}(\boldsymbol{X},\overline{\omega})$ be mappings and sub GRF such that from a finite Karhunen-Loéve expansion $s_k\phi^{s_k}(\boldsymbol{X},\overline{\omega}) = \langle s_k\alpha^{s_k}(\boldsymbol{X}), \xi(\overline{\omega})\rangle_{\mathbb{R}^l}$. Then

$$\begin{aligned}&\mathbb{P}\left\{\sup_{\boldsymbol{X},\overline{\omega}}\left(s_k\phi^{s_k}(\boldsymbol{X},\overline{\omega})\right) \geq s_k u\right\} \approx \mathbb{E}\left\{\varphi\left(\mathcal{A}_{s_k u}\left(s_k\phi^{s_k},\mathcal{T}\right)\right)\right\} \\ &= s_k\mathbb{E}\left\{\varphi\left(\mathcal{A}_u\left(\phi^{s_k},\mathcal{T}\right)\right)\right\} \\ &= \frac{\Gamma(l/2)}{2\pi^{l/2}}\sum\nolimits_{j=0}^{N}\mathbb{E}\left\{\tilde{G}_{j,l}\left(cos^{-1}(u/|\xi|)\right)\boldsymbol{1}_{|\xi|\geq u}\right\} \\ &\quad \times \mathcal{L}_j(s_k\alpha^{s_k}),\end{aligned} \tag{13}$$

where $\tilde{G}_{j,l}(\rho) = \sum_{n=0}^{\lfloor j/2\rfloor}\dfrac{(-4\pi)^{-n}j!}{n!(j-2n)!}G_{j-2n,l-1+2n-j}(\rho)$.

See proof in Appendix.

Let $(\mathcal{T},g)$ be an 2-dimension Riemannian manifold where g is the Riemannian metric tensor. For each $\boldsymbol{X} \in \mathcal{T}$, there is an inner product $g_{\boldsymbol{X}} : T_{\boldsymbol{X}}\mathcal{T} \times T_{\boldsymbol{X}}\mathcal{T} \to \mathbb{R}$ such that $(\xi_{\boldsymbol{X}},\sigma_{\boldsymbol{X}}) \mapsto g_{\boldsymbol{X}}(\xi_{\boldsymbol{X}},\sigma_{\boldsymbol{X}})$ where $T_{\boldsymbol{X}}\mathcal{T}$ is the tangent space of $\mathcal{T}$ at $\boldsymbol{X}$. Let $\langle\xi_{\boldsymbol{X}},\sigma_{\boldsymbol{X}}\rangle$ the inner product $g_{\boldsymbol{X}}(\xi_{\boldsymbol{X}},\sigma_{\boldsymbol{X}})$. For a coordinate system with basis $\left\{\dfrac{\partial}{\partial X_i}|_{\boldsymbol{X}}\right\}_{i=1,2}$ we have for

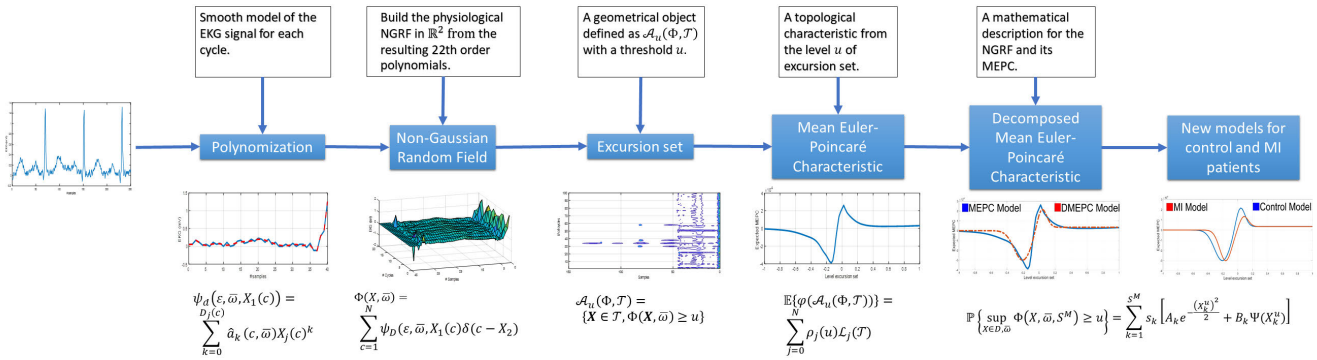

FIGURE 1. Proposed method to model EKG holter.

$$i,j=1,2$$

$$g_{ij}(\boldsymbol{X}) := g_{\boldsymbol{X}}\left(\frac{\partial}{\partial X_i}|_{\boldsymbol{X}}, \frac{\partial}{\partial X_j}|_{\boldsymbol{X}}\right) = \langle \frac{\partial}{\partial X_i}|_{\boldsymbol{X}}, \frac{\partial}{\partial X_j}|_{\boldsymbol{X}}\rangle \tag{14}$$

which are called the components of g at $\boldsymbol{X}$ under this coordinate system. Let $G(\boldsymbol{X}) = \left(g_{ij}(\boldsymbol{X})\right)$ for $i,j = 1,2$ be a symmetric and positive definite matrix from the definition of g. For a real-valued function ϕ on $\mathcal{T}$, let $\phi_i = \frac{\partial}{\partial X_i}\phi$ and $\phi_{ij} = \frac{\partial^2}{\partial X_i \partial X_j}\phi$. Define the length of the differentiable curve $\gamma : [a,b] \to \mathcal{T}$ by $\mathcal{L}(\gamma) = \int_0^1 \sqrt{\langle \gamma'(t)\gamma(t)\rangle}dt$. Then the distance on $\mathcal{T}$ by the Riemannian metric g is $d_{\mathcal{T}}(\boldsymbol{X},\boldsymbol{Y}) = \inf_{\gamma \in D^1([0,1];\mathcal{T})_{\boldsymbol{X},\boldsymbol{Y}}} \mathcal{L}(\gamma)$. Riemannian metric g is closely related to the covariance function $C(\boldsymbol{X},\boldsymbol{Y}) = \mathbb{E}\left\{\phi_p\phi_q\right\}$. In particular for $\boldsymbol{X_0} \in \mathcal{T}$, it follows that

$$g_{\boldsymbol{X_0}} = \xi_{\boldsymbol{X_0}}\sigma_{\boldsymbol{X_0}}C(\boldsymbol{X},\boldsymbol{Y})|_{\boldsymbol{X}=\boldsymbol{Y}=\boldsymbol{X_0}}. \tag{15}$$

Lemma 2: Let $\phi_* = \{\phi_*(\boldsymbol{X},\overline{\omega}), \boldsymbol{X} \in \mathcal{T}, \overline{\omega} \in \overline{\Omega}\}$ be a GRF satisfying $C(\boldsymbol{X},\boldsymbol{Y}) = 1 - cd_{\mathcal{T}}^2(\boldsymbol{X},\boldsymbol{Y})(1+o(1))$, $c>0$, where $(\mathcal{T},g)$ is an 2-dimension Riemannian manifold. Let $D \subset \mathcal{T}$ be an 2-dimension compact submanifold on $\mathcal{T}$. Then,

$$\mathbb{P}\{\sup_{\boldsymbol{X}\in D,\overline{\omega}} \phi_*(\boldsymbol{X},\overline{\omega}) \geq u\} = \sum\nolimits_{j=1}^{m} \mathbb{P}\{\sup_{\boldsymbol{X}\in D_j,\overline{\omega}} \phi_*^j(\boldsymbol{X},\overline{\omega}) \geq u\}, \tag{16}$$

where $D = \cup_{j=1}^m D_j$, $\phi_*^j(\boldsymbol{X},\overline{\omega}) \in D_j$ and $\phi_*(\boldsymbol{X},\overline{\omega}) = (\phi_*^1(\boldsymbol{X},\overline{\omega}),\ldots,\phi_*^m(\boldsymbol{X},\overline{\omega}))$.

See proof in Appendix.

Now we present the main Theorem of our method related to the decomposition of EPC.

Theorem 3: Let $s_j\phi^j(\boldsymbol{X},\overline{\omega})$ be a collection of i.i.d. signed sub GRF. Let $D = \cup_{j=1}^m D_j$ be a composition such that $\phi^j(\boldsymbol{X},\overline{\omega}) \in D_j$. Let $\Phi(\boldsymbol{X},\overline{\omega},S^M) = \left(s_1\phi^{s_1}(\boldsymbol{X},\overline{\omega}),\ldots,s_{S^M}\phi^{s_{S^M}}(\boldsymbol{X},\overline{\omega})\right)$ be a NGRF where $\Sigma_s = (s_1,\ldots s_{S^M})$ with s_j the SUW of each $\phi^{s_j}(\boldsymbol{X},\overline{\omega})$ and $S^M = \sum_{j=1}^M (-1)^j s_j$. Then

$$\mathbb{P}\{\sup_{\boldsymbol{X}\in D,\overline{\omega}} \Phi(\boldsymbol{X},\overline{\omega},S^M) \geq u\}$$

$$= \sum\nolimits_{k=1}^{S^M} s_k\left[A_k\exp(-(X_k^u)^2/2) + B_k\Psi(X_k^u)\right], \tag{17}$$

with $X_k^u = (u-\mu_k)/\sigma_k$, $\mu_k,\sigma_k,A_k,B_k \in \mathbb{R}$, Ψ the tail probability function, and the mother-wave defined as

$$W(X_k^u) = A_k\exp(-(X_k^u)^2/2) + B_k\Psi(X_k^u). \tag{18}$$

See proof in Appendix. Eq.(17) means that all signed decomposed NGRF has a decomposed mean Euler-Poincaré Characteristic. This formula allows to treat complex cases of signal containing outliers such that R waves as shown in experimental data.

III. METHODOLOGY

The MEPC can not be modeled by the classical approach of [1]. Instead, we introduce a decomposed MEPC (DMEPC) based on a *mother-wave* dependent on the excursion set level u, the mean, and the standard deviation of the MEPC. The new DMEPC leads to a simple model, opposite to the more complicated choice of F for NGRFs by the method in [1]. Fig. 1 summarizes the methodology.

A. DATA

EKG is a standard medical test to diagnose cardiovascular conditions. It is well-known that it is indeed feasible to recognize specific cardiac events by analyzing abnormalities in primary waves (PQRST) of a cardiac cycle [27]. We propose to study the behavior pattern of control patients with some cardiac events by assessing the MEPC from the NGRF formed with a RAP model of the P-waves from Holter EKG records. For this study, the EKG data were gathered from the Smart Health for Assessing the Risk of Events (SHAREE) database of PhysioNet [24]. We deal with EKG signals from wearable health monitoring devices. The data spans 139 hypertensive patients. Their EKG signals were digitized at 128 Hz and registered for 24 hours, which means around 94000 cardiac cycles. All patients were followed for 12 months after monitoring to record any cardiac event. In sum, 11 patients suffered myocardial infarctions, 3 of them, stroke, and 3 syncope episodes. Our study held 28 subjects: those with events and 11 control patients among the hypertensive subjects without events. The EKG data handling was set

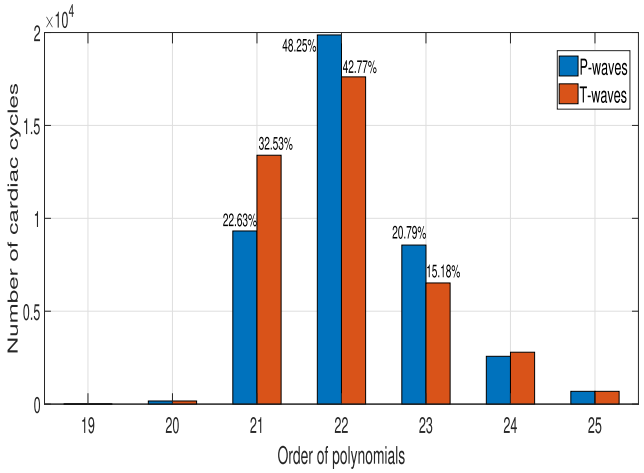

FIGURE 2. Histogram to select the best order of the polynomials P_1 (P-waves) and P_2 (T-waves) for each cardiac cycle.

just to keep P waves. This choice's motivation comes from the fact that P-waves reveal atrial depolarization and have irregular behavior faced with heart events.

B. PRE-PROCESSING OF SIGNALS

Polynomization has been dealt with as follows. A polynomial function was used to match the EKG signal after splitting the cycles into two parts ($j = 1, 2$). To achieve this goal, we begin by detecting in the EKG, the location of the R-peaks $R_k, k = 1, \ldots, N_c$, where N_c is the number of cycles with the algorithm of Pan-Tompkin [28]. Thereupon, we split the cycles by setting a threshold (the middle point m_k between R-points), while keeping in all segments the principal waves, namely, P, R, and T. Every cycle N_c is polynomized covering two intervals $P_1(c) = [m_k, R_{k+1}]$ and $P_2(c) = [R_{k+1}, m_{k+1}]$ in the form of Eq.(1). In the end, one gets polynomials of proper order $D_j(c)$.

To determine the order of the polynomials that gives the best estimation of the measured data, we assessed the Normalized Root Mean Square Error (NRMSE) Eq.(19), as shown at the bottom of the page, where $\bar{P}_j$ is the mean of P_j and the vector of the estimated coefficients $\hat{a}_k$ is computed by the inverse of the Vandermonde matrix [29]. Based on the NRMSE, we looked for the maximum FIT (Eq.(19)) of 40,000 cardiac cycles from 22 patients for both polynomials of every cycle. A frequency histogram plots the relationship between the fit of the polynomials and the orders between 20 and 25 ($D(c) = 20, \ldots, 25$). The result for $P_1(c)$ and $P_2(c)$ are in Fig. 2. In both cases, the order withheld is 22.

From now on, the order of the polynomials is set at $D_1(c) = 22$ and $D_2(c) = 22$. In this way, the polynomials $I_1(c)$ and $I_2(c)$ are obtained in terms of the coefficients P_j. Algorithm 1 dictates the entire procedure. As a result, it returns the structure arrays P_1 and P_2.

Algorithm 1 Algorithm for Calculating Random Algebraic Polynomials

Input: Holter EKG

Output: Polynomials $P_1(c)$ and $P_2(c)$

Initialization;

1: Detect the peaks position R_k, $k = 1, \ldots, N_c$ using the Pan-Tompkin algorithm [28];
2: Detect the middle points $m_k = \frac{R_{k+1}-R_k}{2}, k = 1, \ldots, N_c - 1$;
3: Determine the order of polynomials using the FIT (eq. 19);
4: Calculate the polynomials $I_1(c)$, $c \in [m_k, R_{k+1}]$ and $I_2(c)$, $c \in [R_{k+1}, m_{k+1}]$ using the Vandermonde matrix;
5: Evaluate polynomials and add results at structure array $P_1(c)$ and $P_2(c)$;

C. RANDOM FIELDS AND EXCURSION SET

Random fields are formed by merging all the polynomials of the cardiac cycles. We proposed to manage the RAP from $P_1(c)$ sections, *i.e.* preserving just the P-waves. Excursion set is a main concept in the random field theory, it is defined by Eq.(4), and the level u is well-chosen between the interval $[-1, 1]$. Fig. 3 shows the excursion set for control patients and Fig. 4, the excursion set for patients who suffered an MI, both with $u = 0.1$, where the P-wave and R-peak are separated. For the sake of clarity, they are plotted with a reduced number of data. The Random fields built in this way must be homogeneous. Thus, the empty spaces are filled with zeros. Shortening, Algorithm 2 opens with the measure the size of all the vectors. Next, the maximum value is settled. Lastly, if the polynomial length is smaller than the maximum length, the spaces are filled with zeros.

D. MEAN EULER-POINCARÉ CHARACTERISTIC AND DECOMPOSED MEAN EULER-POINCARÉ CHARACTERISTIC

The EPC $\varphi(\mathcal{A}_u(\Phi, \mathcal{T}))$ of each excursion set was obtained by converting the set into a binary image using the following logic: A value higher than the level u is codified as being 1, and 0 otherwise. The Gray's algorithm [30] performed on the binary image gives the EPC. The EPC is a scalar that stands for the number of elements connected minus the number of holes in those elements [14]. In the next step, the EPC is got for all control and MI patients. To standardize for those many tests, the MEPC is derived, displayed for control patients, and compared with the cases from MI, syncope, and stroke events.

$$FIT = \max \left\{ 100 \left(1 - \frac{\left\| P_j(c) - \sum_{k=0}^{D_j(c)} \hat{a}_k(c, \bar{\omega}) X_j(c)^k \right\|}{\left\| P_j(c) - \bar{P}_j(c) \right\|} \right) \right\}_{j=1,2.} \tag{19}$$

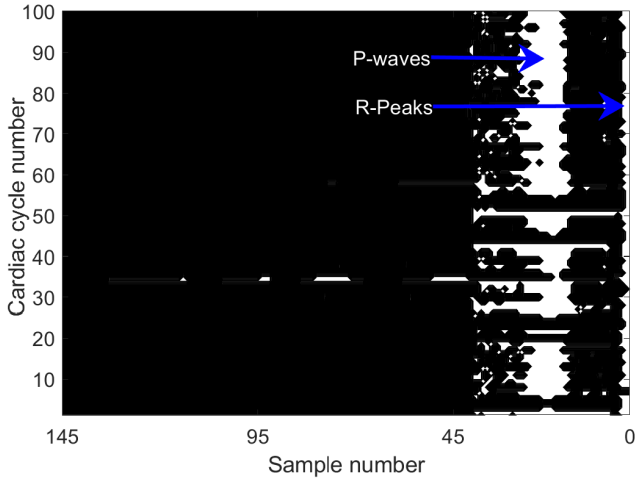

FIGURE 3. Excursion set of the Non-Gaussian Random Field at $u = 0.1$ for a control patient's P-waves.

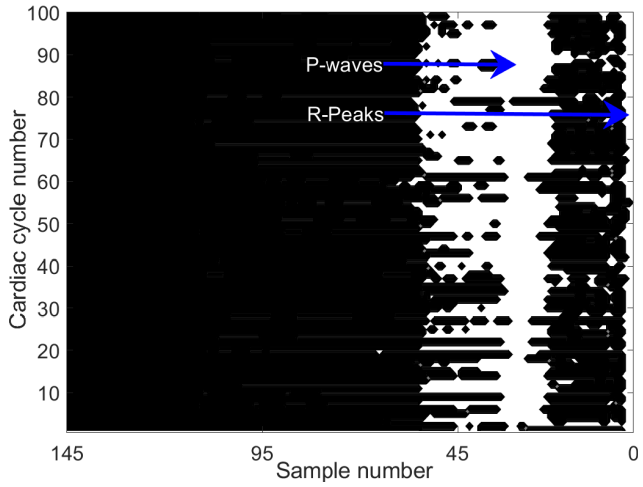

FIGURE 4. Excursion set of the Non-Gaussian Random Field at $u = 0.1$ for a MI patient's P-waves.

Finally, We used the DMEPC model from Eq. (17) based on the mother-wave defined in Eq. (18) to get the models; the parameters were estimated using the PSO algorithm [31], and the results are in Tables 1 to 4.

IV. RESULTS AND DISCUSSION

To standardize the different cardiopathy events, we calculated the average of the MEPC for each group: 11 control patients, 11 MI patients, 3 syncope cases and 3 stroke cases. The result is in Fig. 9. make it evident that the EKG treated signals cannot be described by the classical GRF model in [1, p. 294], Eqs. (7, 11, 14. So, we use our DMEPC method to describe these NGRF. The results are given in Fig. 8 and Tables 1 to 4. We show the parameters obtained based on the PSO algorithm. The FIT (Eq. (19)) is the chosen indicator to settle the best match between the estimated and the measured MEPC. The DMEPC models meet 65% to 81%.

Algorithm 2 Algorithm to Build the non-Gaussian Random Field

Input: Polynomials $P_1(c)$ and $P_2(c)$

Output: *Non-Gaussian Random Field* $\Phi(X, \bar{\omega}, S^M)$

Initialization;

for $k = 1\ N_c$ **do**
  $A(k) = length(P_l(c)_k), l = 1, 2$
end for
$M = \max\{A\} | M \in \mathbb{R}$
if $(A_k < M)$ **then**
  $\Phi_1([k, 1 : M], \bar{\omega}, S^M) = [zeros, P_1(c)_k]$ and $\Phi_2([k, 1 : M], \bar{\omega}, S^M) = [P_2(c)_k, zeros]$
else
  $\Phi_1([k, 1 : M], \bar{\omega}, S^M) = P_1(c)_k$ and $\Phi_2([k, 1 : M], \bar{\omega}, S^M) = P_2(c)_k$
end if
Calculate the level u of excursion sets: $u = [u_1 : (u_n - u_1)/N_u : u_n]$, where $u_1 = \min\{\Phi(X, \bar{\omega}, S^M)\}$, $u_n = \max\{\Phi(X, \bar{\omega}, S^M)\}$,and N_u=number of levels;

Algorithm 3 Algorithm to Get the Values of Mean Euler-Poincaré Characteristic From *Excursion Set*

Input: *Non-Gaussian Random Field* $\Phi(X, \bar{\omega}, S^M)$,*u (level)*

Output: *Euler-Poincaré Characteristic* $\varphi(\mathcal{A}_u)$

Initialization;

for $k = 1$ to N_c **do**
  for $j = 1$ to M **do**
    if $(\Phi([k, j], \bar{\omega}, S^M) >= \mu)$ **then**
      $\mathcal{A}_u(k, j) = 1$
    else
      $\mathcal{A}_u(k, j) = 0$
    end if
  end for
end for
$\varphi(\mathcal{A}_u) = \frac{1}{4}[n\{Q_1\} - n\{Q_3\} + 2n\{Q_D\}]$

TABLE 1. Parameters for the MI models.

Model	FIT	k	A	B	σ	μ
MI 1	77%	1	-65211.07	476.1843	0.089	-0.173
		2	33858.71	4130.40	0.056	0.065
MI 2	73%	1	-64230.47	513.4826	0.073	-0.141
		2	29872.87	2246.857	0.049	0.051
MI 3	72%	1	-74014.29	809.90	0.101	-0.202
		2	45085.14	10765.96	0.048	0.057
MI 4	72%	1	-58996.29	877.56	0.127	-0.200
		2	38491.64	5014.94	0.090	0.115
MI 5	78%	1	35731.51	6213.03	0.075	0.099
		2	-52232.17	246.88	0.062	-0.110
		3	-29548.24	363.37	0.110	-0.340
MI 6	65%	1	-85156.30	867.54	0.076	-0.091
		2	45424.63	8843.88	0.056	0.076

Fig. 5 shows the comparison between the average of the MEPC control patients and MI patients. The MEPC of the MI patients differs from the control MEPC curve in its amplitude. The Euler characteristic distribution for MI patients

TABLE 2. Parameters for the syncope models.

Model	FIT	k	A	B	σ	μ
Syncope 1	76%	1	-32686.33	50.88	0.057	0.016
		2	23019.93	5427.64	0.04	0.189
Syncope 2	74%	1	-18907.67	281.21	0.099	-0.02
		2	24857.1	144.1	0.042	0.179
		3	12523.71	3517.81	0.116	0.506
Syncope 3	81%	1	-39960.47	142.21	0.046	0.036
		2	31070.26	1384.91	0.045	0.194

TABLE 3. Parameters for the stroke models.

Model	FIT	k	A	B	σ	μ
Stroke 1	79%	1	-48441.39	183.59	0.041	0.067
		2	35719.09	1025.19	0.043	0.201
		3	6138.78	1786.5	0.072	0.829
Stroke 2	74%	1	-46420.87	458.39	0.077	0.02
		2	37937.06	3746.21	0.067	0.239
Stroke 3	60%	1	-17973.33	-228.9	0.091	-0.053
		2	26010.7	876.06	0.069	0.117

TABLE 4. Parameters for the mean DMEPC models.

Model DMEPC	FIT	k	A	B	σ	μ
Control	77%	1	-38940.19	560.41	0.104	-0.195
		2	28017.40	16613.80	0.065	0.075
MI	71%	1	-58392.27	755.79	0.108	-0.166
		2	37425.67	6204.29	0.062	0.078
Stroke	78%	1	-34871.91	175.72	0.073	-0.008
		2	27881.90	3599.18	0.053	0.211
Syncope	77%	1	-29566.22	202.83	0.059	0.019
		2	25297.32	5121.67	0.038	0.183

changes compared with that of the control group, concentrating more on negative values. A more pronounced reduction is observed, with a more prominent MEPC minimum and a slightly smaller maximum. A certain regularity in shape is to be noticed for all MI patients. The DMEPC model gives different traces for MI patients, compared with the control patients. We decomposed the MI MEPC using Eq. (18) with $S^M = 2$, except for the fifth MI patient; for this case, we used $S^M = 3$. Table 1 shows the parameter for each S^M. These values are achieved with algorithm 4. The particles ρ are for the parameters A, B, μ, and σ of Eq. (18). In this equation, the cost function CJ is the maximum fit that the estimate of the parameters attains. Accordingly, the values recorded are the maximum reached under the given restrictions by the outlined method.

Figs. 6 and 7 show the average model of control patients versus syncope and stroke DMEPC models, respectively. The deviation from the average DMEPC of control patients is evident for both heart conditions. They differ in amplitude, though more noticeable is a shift to the right. The displacement of the curves is more or less consistent, making it possible to recognize a quite definite pattern. Larger-scale research will further confirm this result and fit the patterns more precisely. The identified patterns are a promising outcome that lets us assert that the DMEPC model of Holter signals can become an auxiliary diagnosis tool for health professionals. Besides, it is worthy to note that a complete EKG of a single subject includes 94000 cycles. The DMEPC model condenses

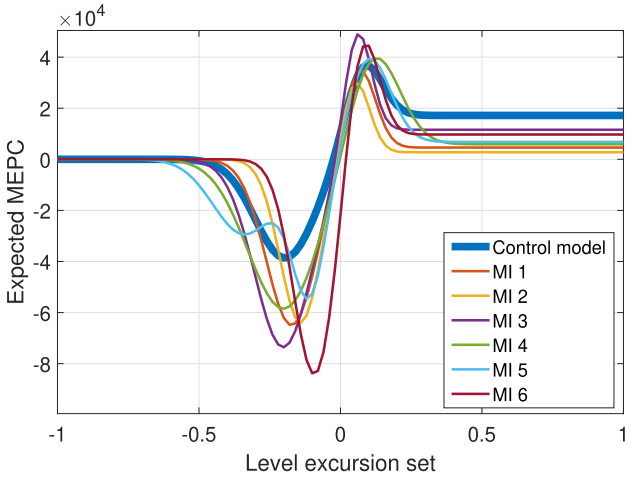

FIGURE 5. A comparison beetween the DMEPC of control patients vs. the DMEPC model for each MI patient.

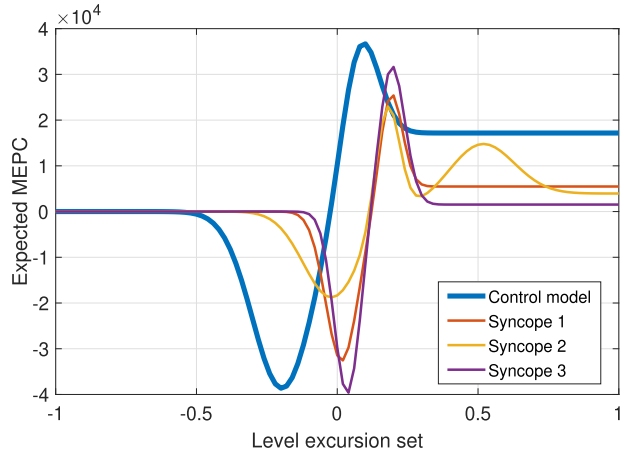

FIGURE 6. A comparison beetween the DMEPC of control patients vs. the DMEPC model of syncope patients.

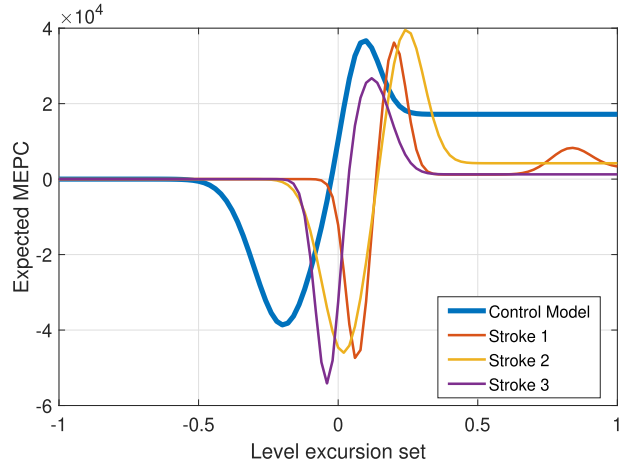

FIGURE 7. A comparison beetween the DMEPC of control patients vs. the DMEPC model of stroke patient.

this data into a simple curve. It stores essential knowledge of the complete Holter record but can be interpreted more easily.

Table 2 and Table 3 give the parameters estimate for the syncope and stoke DMEPC models. To estimate them,

Algorithm 4 Algorithm for Get the Parameters of the Decomposed Mean Euler-Poincaré Characteristic Model Using PSO

Input: *Mean Euler-Poincaré Characteristic* $\mathbb{E}\{\varphi(Au)\}$
Output: $A_k, B_k, C_k, \sigma_k, \mu_k$ parameters
Initialization:

1: Initialize velocity w, c_1 and c_2 constants, and define the cost function CJ
2: Select the number of particles N_p and create random particles $\rho(4, N_p)$ using the constraints for each parameter and random velocities $V(4, N_p)$
3: Calculate the fitness of each particle (F_p)
4: If $F_p > pBest$ in the iteration so the set of values of F_p is the new $pBest$
5: Choose the particle with the best $CJ = 100\left(\frac{\|y-\hat{y}\|}{\|y-\bar{y}\|}\right)$ of all the particle as the $gBest$
6: Calculate particle velocity using

$$V = \omega V + c_1(pBest - \rho) + c_2(gBest - \rho), \quad (20)$$

where $c_1, c_2 \in \mathbb{R}$, V = velocity of the particle and ρ = particle
7: Update particle position with

$$\rho = \rho + V \quad (21)$$

8: Update particle using the next constraints:
- $-100000 <= A_k <= 100000$
- $-100000 <= B_k <= 100000$
- $-1 <= \mu <= 1$
- $0 <= \sigma <= 1$

9: When the number of maximum iterations or maximum fit is accomplished, the approximate solution is the particle with best fitness and STOP; contrarily add iteration and turn to 3.

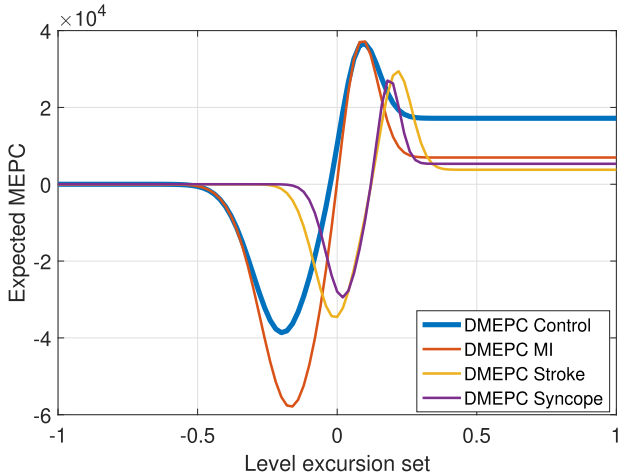

FIGURE 8. A representation of the MEPC based on DMEPC for the four cases (control MI, syncope, and stroke).

we used Algorithm 4 with proper restraints. We distinguished some irregular patterns for each event (Syncope 2 and Stroke 1), where $S^M = 3$ instead of 2. These describe an

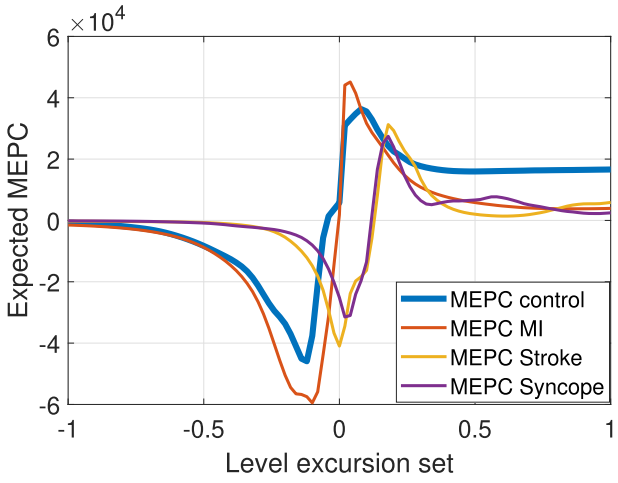

FIGURE 9. The MEPC for each kind of cases (Control, MI, Syncope, and Stroke).

EPC distribution change, as more connected components than holes are observed at different levels u for syncope and stroke incidents. Conversely, for MI episodes (MI 5), holes become more than connected components at different levels u. These features can be seen in the figures as oscillations arise over negative incursion levels for MI DMEPC. Then over positive incursion levels for syncope and stroke DMEPC.

V. CONCLUSION

This paper highlights a new method of the mean Euler-Poincaré characteristic based on a decomposition of an NGRF to elementary GRF related to a *mother-wave*. The theory, along with the mathematical structure, has been outlined. Then these were applied to model myocardial infarction, stroke and syncope from Holter EKG records. The results prove the flexibility of the proposed method for explaining the behavior of the MEPC from NGRF. Future researches should concern issues on the classification of myocardial infarction based on long-term data, with the aim of giving insights into a medical diagnosis.

APPENDIX

A. PROOF OF LEMMA 2.1

Define two sets such that

$$\mathcal{E}_u^{s_{2n+1}}(\mathcal{T}) = \left\{ \boldsymbol{X} \in \mathcal{T}, \overline{\omega} \in \Omega : \inf_{\boldsymbol{X},\overline{\omega}} \phi^{s_{2n+1}}(\boldsymbol{X}, \overline{\omega}) \leq u \right\} \quad (22)$$

$$\mathcal{E}_u^{s_{2n}}(\mathcal{T}) = \left\{ \boldsymbol{X} \in \mathcal{T}, \overline{\omega} \in \Omega : \sup_{\boldsymbol{X},\overline{\omega}} \phi^{s_{2n}}(\boldsymbol{X}, \overline{\omega}) \geq u \right\} \quad (23)$$

Using a Karhunen-Loéve expanding of $\phi^{s_k}(\boldsymbol{X}, \overline{\omega})$

$$\mathbb{P}\left\{ \sup_{\boldsymbol{X},\overline{\omega}} (s_k \phi^{s_k}(\boldsymbol{X}, \overline{\omega})) \geq s_k u \right\}$$

$$= \int_u^{\infty} \mathbb{P}\left\{ \sup_{\boldsymbol{X},\overline{\omega}} \left\langle s_k \alpha^{s_k}(\boldsymbol{X}), \xi(\overline{\omega}) \right\rangle \right.$$

$$
\begin{aligned}
&\geq s_k u|, |\xi(\overline{\omega})| = r\Big\}\mathbb{P}_{|\xi(\overline{\omega})|}(dr) \\
&= \int_u^{\infty} \mathbb{P}\left\{\sup_{\boldsymbol{X},\overline{\omega}} \left\langle s_k \alpha^{s_k}(\boldsymbol{X}), \xi(\overline{\omega})/r\right\rangle\right. \\
&\quad \geq (s_k u/r)|, |\xi(\overline{\omega})| = r\Big\}\mathbb{P}_{|\xi(\overline{\omega})|}(dr) \\
&= \int_u^{\infty} \eta_l(\text{Tube}(s_k \alpha^{s_k}(\mathcal{T}), cos^{-1}(s_k u/r)))\mathbb{P}_{|\xi(\overline{\omega})|}(dr)
\end{aligned} \tag{24}
$$

Remember that $\eta_l\,(Tube\,(A,\rho))\,s_N = \mathcal{H}_{l-1}\,(Tube\,(A,\rho))$ with $s_N = 2\pi^{l/2}/\,\Gamma(l/2)$, we then get

$$
\begin{aligned}
&\mathbb{P}\left\{\sup_{\boldsymbol{X},\overline{\omega}}(s_k \phi^{s_k}(\boldsymbol{X},\overline{\omega})) \geq s_k u\right\} \\
&= \frac{\Gamma(l/2)}{2\pi^{l/2}} \int_u^{\infty} \mathcal{H}_{l-1}\left(Tube\left(s_k \alpha^{s_k}(\mathcal{T}), \cos^{-1}\left(\frac{s_k u}{|\,\xi(\overline{\omega})\,|}\right)\right)\right)\mathbb{P}_{|\xi(\overline{\omega})|}(dr) \\
&= \frac{\Gamma(l/2)}{2\pi^{l/2}} \mathbb{E}\left\{\mathcal{H}_{l-1}\left(Tube\left(s_k \alpha^{s_k}(\mathcal{T}), cos^{-1}\left(\frac{s_k u}{r}\right)\right)\right)\mathbf{1}_{\xi(\overline{\omega})\geq s_k u}\right\}
\end{aligned}
$$

with

$$
\begin{aligned}
&\mathcal{H}_{l-1}\left(Tube\left(s_k \alpha^{s_k}(\mathcal{T}), cos^{-1}\left(\frac{u}{\xi(\overline{\omega})}\right)\right)\right) \\
&\qquad \approx \sum_{j=0}^{N} \tilde{G}_{j,l}\left(cos^{-1}\left(\frac{u}{|\xi\overline{\omega}|}\right)\right)\mathcal{L}_j(s_k \alpha^{s_k}(\mathcal{T})),
\end{aligned}
$$

and $\mathcal{L}_j(s_k f(\mathcal{T})) = (s_k)^{N-1}\mathcal{L}_j(f(\mathcal{T}))$, from [15]

$$
\begin{aligned}
&\mathbb{P}\left\{\sup_{\boldsymbol{X},\overline{\omega}}(s_k \phi^{s_k}(\boldsymbol{X},\overline{\omega})) \geq s_k u\right\} \\
&\quad = s_k \frac{\Gamma(l/2)}{2\pi^{l/2}} \sum_{j=0}^{N} \mathbb{E}\left\{\tilde{G}_{j,l}\left(cos^{-1}\left(\frac{u}{|\xi(\overline{\omega})|}\right)\right)\mathbf{1}_{\xi(\overline{\omega})\geq u}\right\} \\
&\quad \times \mathcal{L}_j(\alpha^{s_k}(\mathcal{T}))
\end{aligned} \tag{25}
$$

Finally

$$
\mathbb{P}\left\{\sup_{\boldsymbol{X},\overline{\omega}}(s_k \phi^{s_k}(\boldsymbol{X},\overline{\omega})) \geq s_k u\right\} \approx s_k \mathbb{E}\left\{\varphi\left(\mathcal{A}_u\left(\phi^{s_k}, \mathcal{T}\right)\right)\right\}
$$

which proves the Lemma.

B. PROOF OF LEMMA 2.2

Let $p, q \in U \subset \mathcal{T}$, where $\boldsymbol{X}$ is fixed and $(U, \mathcal{T})$ is a chart of $\mathcal{T}$. Then

$$
d^2_{\mathcal{T}}(p,q) = \sum_{i,j=1}^{2} g_{i,j}(p)(X_i(q) - X_i(p))(X_j(q) - X_j(p)) \tag{26}
$$

Let $\gamma : [0,1] \to \mathcal{T}$ be a curve on $\mathcal{T}$ such that $\gamma(0) = p$ and $\gamma([0,1]) \subset U$. For $\delta > 0$, let $L(\gamma([0,1]))$ be the length of the segment between $\gamma(0)$ and $\gamma(\delta)$. Thus $\gamma'(t) = \sum_{i=1}^{2} \frac{dX_i(\gamma(t))}{dt}\frac{\partial}{\partial X_i}$ and

$$
\begin{aligned}
&L(\gamma[0,1]) \\
&\quad = \int_0^{delta} \sqrt{g_{\gamma(t)}(\gamma'(t),\gamma'(t))}dt \\
&\quad = \int_0^{\delta} \left(\sum_{i,j=1}^{2} g_{ij}(\gamma(t))\frac{dX_i(\gamma(t))}{dt}\frac{dX_j(\gamma(t))}{dt}\right)^{\frac{1}{2}} dt \\
&\quad = \left(g_{i,j}(p)(X_i(q) - X_i(p))(X_j(q) - X_j(p))\right)^{\frac{1}{2}} \\
&\quad = \| \, G^{\frac{1}{2}}(p) \cdot (\varphi(q) - \varphi(p)) \, \|
\end{aligned} \tag{27}
$$

Then we conclude that $d_{\mathcal{T}}(\boldsymbol{X},\boldsymbol{Y}) = \| \, G^{\frac{1}{2}}(\boldsymbol{X}) \cdot (\varphi(\boldsymbol{Y}) - \varphi(\boldsymbol{X})) \, \|$ for $\boldsymbol{X}, \boldsymbol{Y} \in U \subset \mathcal{T}$. Let (U_i, φ_i) be an atlas of $\mathcal{T}$ where $\varphi : U \mapsto \varphi(U) \subset \mathbb{R}^2$ is a homeomorphism. Since D is compact, it has a finite covering $(U_i, \varphi_i)_{i\in I_0}$ where $I_0 \subset I$ is a finite index set. For $i \in I_0$, define $\tilde{\phi} : \varphi_i(U_i) \subset \mathbb{R}^2 \to \mathbb{R}^2$ by $\tilde{\phi} = \phi \circ \varphi_i^{-1}$. From about result, the covariance function of $\tilde{\phi}$ can then written as

$$
\begin{aligned}
&\tilde{C}(\varphi_i(\boldsymbol{X}), \varphi_i(\boldsymbol{Y})) \\
&= 1 - c \, \| \, (G^{\frac{1}{2}} \circ \varphi_i^{-1})(\varphi_i(\boldsymbol{X})(\varphi_i(\boldsymbol{X}) - \varphi_i(\boldsymbol{Y})) \, \|^2 \, (1 + o(1)) \\
&= 1 - \| \, c^{\frac{1}{2}}(G^{\frac{1}{2}} \circ \varphi_i^{-1})(\varphi_i(\boldsymbol{X})(\varphi_i(\boldsymbol{X}) - \varphi_i(\boldsymbol{Y})) \, \|^2 \, (1 + o(1))
\end{aligned} \tag{28}
$$

Making a decomposition $D = \cup_{j=1}^{m} D_j$ where $D \subset \mathcal{T}$ then

$$
\begin{aligned}
&\mathbb{P}\left\{\sup_{\boldsymbol{X}\in D_j,\overline{\omega}} \phi(\boldsymbol{X},\overline{\omega}) \geq u\right\} \\
&\quad = \mathbb{P}\left\{\sup_{\tilde{\boldsymbol{X}}\in\varphi_i(D_j),\overline{\omega}} \tilde{\phi}(\boldsymbol{X},\overline{\omega}) \geq u\right\} \\
&\quad = \left(\int_{\varphi_i(D_j)} |det\left(c^{\frac{1}{2}}(G^{\frac{1}{2}} \circ \varphi_i^{-1})(\tilde{\boldsymbol{X}})\right)|d\tilde{\boldsymbol{X}}\right) \\
&\qquad \times H_{2,2} u^2 \Psi(u)(1 + o(1)) \\
&\quad = \left(\int_{\varphi_i(D_j)} |det\left((G \circ \varphi_i^{-1})(\tilde{\boldsymbol{X}})\right)|^{\frac{1}{2}} d\tilde{\boldsymbol{X}}\right) \\
&\qquad \times c H_{2,2} u^2 \Psi(u)(1 + o(1)) \\
&\quad = Vol(D_j) c H_{2,2} u^2 \Psi(u)(1 + o(1)),
\end{aligned} \tag{29}
$$

where $H_{2,2}$ is the Pickands' constant in $\mathbb{R}^2$ defined by

$$
H_{2,2} = \lim_{K\to\infty} \frac{1}{K^2} \int_0^{\infty} e^u \mathbb{P}\left\{\sup_{\boldsymbol{Y}\in[0,K]^2,\overline{\omega}} Z(\boldsymbol{Y},\overline{\omega}) \geq u\right\} du
$$

On the other hand, from $D = \cup_{j=1}^{m} D_j$ and $\phi^j(\boldsymbol{X},\overline{\omega}) \in D_j$ using a NGRF set given by $\phi(\boldsymbol{X},\overline{\omega}) = (\phi^1(\boldsymbol{X},\overline{\omega}), \ldots, \phi^m(\boldsymbol{X},\overline{\omega}))$

$$
\mathbb{P}\left\{\sup_{\boldsymbol{X}\in D,\overline{\omega}} \phi(\boldsymbol{X},\overline{\omega}) \geq u\right\} \leq \sum_{j=1}^{m} \mathbb{P}\left\{\sup_{\boldsymbol{X}\in D_j,\overline{\omega}} \phi^j(\boldsymbol{X},\overline{\omega}) \geq u\right\}
$$

By the Bonferroni inequality

$$\mathbb{P}\left\{\sup_{\boldsymbol{X}\in D,\overline{\omega}}\phi(\boldsymbol{X},\overline{\omega})\geq u\right\}\geq\sum_{j=1}^{m}\mathbb{P}\left\{\sup_{\boldsymbol{X}\in D_j,\overline{\omega}}\phi^j(\boldsymbol{X},\overline{\omega})\geq u\right\}$$
$$-\sum_{j\neq j'}\mathbb{P}\left\{\sup_{\boldsymbol{X}\in D_j,\overline{\omega}}\phi^j(\boldsymbol{X},\overline{\omega})\geq u,\ \sup_{\boldsymbol{Y}\in D_{j'},\overline{\omega}}\phi^{j'}(\boldsymbol{Y},\overline{\omega})\geq u\right\}. \tag{30}$$

If D_j and $D_{j'}$ are not adjacent, i.e. $d_{\mathcal{T}}>0$, then from the Borell-TIS inequality

$$\lim_{u\to\infty}\frac{\mathbb{P}\left\{\sup_{\boldsymbol{X}\in D_j,\overline{\omega}}\phi^j(\boldsymbol{X},\overline{\omega})\geq u,\ \sup_{\boldsymbol{Y}\in D_{j'},\overline{\omega}}\phi^{j'}(\boldsymbol{Y},\overline{\omega})\geq u\right\}}{u^2\Psi(u)}$$
$$\leq\lim_{u\to\infty}\frac{\mathbb{P}\left\{\sup_{\boldsymbol{X}\in D_j,\boldsymbol{Y}\in D_{j'},\overline{\omega}}\left[\frac{\phi^j(\boldsymbol{X},\overline{\omega})+\phi^{j'}(\boldsymbol{Y},\overline{\omega})}{2}\right]\geq u\right\}}{u^2\Psi(u)}$$
$$=0.$$

If D_j and $D_{j'}$ are adjacent, there exists a chart (U_i,φ_i) containing both D_j and $D_{j'}$. Therefore

$$\mathbb{P}\left\{\sup_{\boldsymbol{X}\in D_j,\overline{\omega}}\phi^j(\boldsymbol{X},\overline{\omega})\geq u,\ \sup_{\boldsymbol{Y}\in D_{j'},\overline{\omega}}\phi^{j'}(\boldsymbol{Y},\overline{\omega})\geq u\right\}$$
$$=\mathbb{P}\left\{\sup_{\boldsymbol{X}\in D_j,\overline{\omega}}\phi^j(\boldsymbol{X},\overline{\omega})\geq u\right\}+\mathbb{P}\left\{\sup_{\boldsymbol{Y}\in D_{j'},\overline{\omega}}\phi^{j'}(\boldsymbol{Y},\overline{\omega})\geq u\right\}$$
$$-\mathbb{P}\left\{\sup_{\boldsymbol{X}\in D_j\cup D_{j'},\overline{\omega}}\phi(\boldsymbol{X},\overline{\omega})\geq u\right\}.$$

By applying Eq.(29) to the last three terms in the previous equation, the joint excursion probability is $o(u^2\Psi(u))$. Thus the last term in Eq.(30) is $o(u^2\Psi(u))$. Finally

$$\sum_{j=1}^{m}\mathbb{P}\left\{\sup_{\boldsymbol{X}\in D_j,\overline{\omega}}\phi^j(\boldsymbol{X},\overline{\omega})\geq u\right\}$$
$$\leq\mathbb{P}\left\{\sup_{\boldsymbol{X}\in D,\overline{\omega}}\phi(\boldsymbol{X},\overline{\omega})\geq u\right\}$$
$$\leq\sum_{j=1}^{m}\mathbb{P}\left\{\sup_{\boldsymbol{X}\in D_j,\overline{\omega}}\phi^j(\boldsymbol{X},\overline{\omega})\geq u\right\}, \tag{31}$$

which proves Lemma.

C. PROOF OF THEOREM 2.1

From Lemma 1, setting $m=S^M$ and $\Phi(\boldsymbol{X},\overline{\omega})=(s_1\phi^{s_1}(\boldsymbol{X},\overline{\omega}),\ldots,s_m\phi^{s_m}(\boldsymbol{X},\overline{\omega}))$, we get

$$\mathbb{P}\left\{\sup_{\boldsymbol{X}\in D,\overline{\omega}}\Phi(\boldsymbol{X},\overline{\omega})\geq u\right\}=\sum_{j=1}^{S^M}\mathbb{P}\left\{\sup_{\boldsymbol{X}\in D_j,\overline{\omega}}(s_j\phi^j(\boldsymbol{X},\overline{\omega}))\geq u\right\}. \tag{32}$$

From Lemma 1, it follows that

$$\mathbb{P}\left\{\sup_{\boldsymbol{X}\in D,\overline{\omega}}\Phi(\boldsymbol{X},\overline{\omega})\geq u\right\}=\sum_{j=1}^{S^M}s_j\mathbb{E}\left\{\varphi\left(\mathcal{A}_u\left(\phi^{s_j},\mathcal{T}\right)\right)\right\}. \tag{33}$$

Using Chapter 14 in [1] for $N=2$ and for centered sub GRF with $X_j^u=\dfrac{u-\mu_j}{\sigma_j}$, it follows that

$$\mathbb{E}\left\{\varphi\left(\mathcal{A}_u\left(\phi^{s_j},\mathcal{T}\right)\right)\right\}=A_j\exp(-(X_j^u)^2/2)+B_j\Psi(X_j^u), \tag{34}$$

which proves Theorem.

REFERENCES

[1] R. J. Adler and J. E. Taylor, *Random Fields and Geometry*, 1st ed. New York, NY, USA: Springer-Verlag, 2007.
[2] C. Sutton and A. McCallum, "An introduction to conditional random fields," *Found. Trends Mach. Learn.*, vol. 4, no. 4, pp. 267–373, 2012.
[3] E. Vanmarcke, *Random Fields: Analysis and Synthesis*. Cambridge, MA, USA: MIT Press, 1983.
[4] R. J. Adler, G. Samorodnitsky, and J. E. Taylor, "High level excursion set geometry for non-Gaussian infinitely divisible random fields," *Ann. Probab.*, vol. 41, no. 1, pp. 134–169, Jan. 2013.
[5] J. Potthoff, "Sample properties of random fields III: Differentiability," *Commun. Stochastic Anal.*, vol. 4, no. 3, p. 3, Sep. 2010.
[6] P. Abrahamsen, *A Review of Gaussian Random Fields and Correlation Functions*. Oslo, Norway: Norwegian Computing Center, Apr. 1997.
[7] R. A. Shaikh, J.-P. Li, A. Khan, and I. Memon, "Biomedical image processing and analysis using Markov random fields," in *Proc. 12th Int. Comput. Conf. Wavelet Act. Media Technol. Inf. Process. (ICCWAMTIP)*, Dec. 2015, pp. 179–183.
[8] G. Zhang, S. Tzoumas, K. Cheng, F. Liu, J. Liu, J. Luo, J. Bai, and L. Xing, "Generalized adaptive Gaussian Markov random field for X-ray luminescence computed tomography," *IEEE Trans. Biomed. Eng.*, vol. 65, no. 9, pp. 2130–2133, Sep. 2018.
[9] R. Bansal, L. H. Staib, D. Xu, H. Zhu, and B. S. Peterson, "Statistical analyses of brain surfaces using Gaussian random fields on 2-D manifolds," *IEEE Trans. Med. Imag.*, vol. 26, no. 1, pp. 46–57, Jan. 2007.
[10] M. A. R. Ferreira and V. De Oliveira, "Bayesian reference analysis for Gaussian Markov random fields," *J. Multivariate Anal.*, vol. 98, no. 4, pp. 789–812, Apr. 2007.
[11] K. J. Worsley, "Boundary corrections for the expected Euler characteristic of excursion sets of random fields, with an application to astrophysics," *Adv. Appl. Prob.*, vol. 27, no. 27, pp. 943–959, Dec. 1995.
[12] K. J. Worsley, "The geometry of random images," *Chance*, vol. 9, no. 1, pp. 27–40, Jan. 1996.
[13] K. Worsley, "Random field theory," in *Statistical Parametric Mapping*, K. Friston, J. Ashburner, S. Kiebel, T. Nichols, and W. Penny, Eds. London, U.K.: Elsevier, 2007, ch. 18, pp. 232–236.
[14] E. Richardson and M. Werman, "Efficient classification using the Euler characteristic," *Pattern Recognit. Lett.*, vol. 49, pp. 99–106, Nov. 2014.
[15] K. J. Worsley, "Local maxima and the expected Euler characteristic of excursion sets of χ^2, F and t fields," *Adv. Appl. Probab.*, vol. 26, no. 1, pp. 13–42, Mar. 1994.
[16] A. T. Bharucha-Reid and M. Sambandham, *Random Polynomials: Probability and Mathematical Statistics: A Series of Monographs and Textbooks*. New York, NY, USA: Academic, 1986.
[17] M. Kac, "On the average number of real roots of a random algebraic equation (II)," *Proc. London Math. Soc.*, vols. 2–50, no. 1, pp. 390–408, 1948.
[18] A. Edelman and E. Kostlan, "The road from Kac's matrix to Kac's random polynomials," in *Proc. SIAM Appl. Linear Algebra Conf.*, Philadelphia, PA, USA, 1994, pp. 503–507.
[19] L. A. Shepp and R. J. Vanderbei, "The complex zeros of random polynomials," *Trans. Amer. Math. Soc.*, vol. 347, no. 11, pp. 4365–4384, Nov. 1995.
[20] C. P. Hughes and A. Nikeghbali, "The zeros of random polynomials cluster uniformly near the unit circle," *Compositio Mathematica*, vol. 144, no. 3, pp. 734–746, May 2008.
[21] E. Durand, *Solutions Numériques des Équations Algébriques (Tome I)*. Paris, France: Masson, 1960.
[22] I. O. Kerner, "Ein gesamtschrittverfahren zur Berechnung der nullstellen von polynomen," *Numerische Math.*, vol. 8, no. 3, pp. 290–294, May 1966.
[23] B. T. Smith, "Error bounds for zeros of a polynomial based upon Gerschgorin's theorems," *J. ACM*, vol. 17, no. 4, pp. 661–674, Oct. 1970.

[24] A. L. Goldberger, L. A. N. Amaral, L. Glass, J. M. Hausdorff, P. C. Ivanov, R. G. Mark, J. E. Mietus, G. B. Moody, C.-K. Peng, and H. E. Stanley, "PhysioBank, PhysioToolkit, and PhysioNet: Components of a new research resource for complex physiologic signals," *Circulation*, vol. 101, no. 23, pp. e215–e220, Jun. 2000.
[25] D. E. Knuth, "Two notes on notation," *Amer. Math. Monthly*, vol. 99, no. 5, pp. 403–422, May 1992.
[26] K. J. Worsley, "Estimating the number of peaks in a random field using the Hadwiger characteristic of excursion sets, with applications to medical images," *Ann. Statist.*, vol. 23, no. 2, pp. 640–669, Apr. 1995.
[27] M. Rosiak, H. Bolinska, and J. Ruta, "P wave dispersion and P wave duration on SAECG in predicting atrial fibrillation in patients with acute myocardial infarction," *Ann. Noninvasive Electrocardiol.*, vol. 7, no. 4, pp. 363–368, Oct. 2002.
[28] J. Pan and W. J. Tompkins, "A real-time QRS detection algorithm," *IEEE Trans. Biomed. Eng.*, vol. BME-32, no. 3, pp. 230–236, Mar. 1985.
[29] A. Klinger, "The vandermonde matrix," *Amer. Math. Monthly*, vol. 74, no. 5, pp. 571–574, 1967.
[30] S. B. Gray, "Local properties of binary images in two dimensions," *IEEE Trans. Comput.*, vols. C–20, no. 5, pp. 551–561, May 1971.
[31] K. Zhang, "A minimum zone method for evaluating straightness errors using pso algorithm," in *Advanced Intelligent Computing Theories and Applications. With Aspects of Theoretical and Methodological Issues*, D.-S. Huang, D. C. Wunsch, D. S. Levine, and K.-H. Jo, Eds. Berlin, Germany: Springer, 2008, pp. 308–314.

MOISES RAMOS-MARTINEZ was born in San Cristobal de Las Casas, Chiapas, Mexico, in 1991. He received the bachelor's degree in mechatronics engineering from Chiapas Polytechnic University, Mexico, in 2013, and the M.Sc. degree in electronic engineering from the National Research and Technological Development Center (CENIDET), Mexico, in 2016, where he is currently pursuing the Ph.D. degree in automatic control.

CHRISTOPHE CORBIER received the Ph.D. degree from the Arts et Métiers Paris-Tech Institute, in 2012. He is currently an Assistant Professor with the Networks and Telecommunications Department, Jean Monnet St-Etienne University. His research focuses on information geometry, non-gaussian random fields, and robust statistics. He has published more than 25 peer-reviewed journal articles, and one chapter in related areas.

VICTOR M. ALVARADO received the Ph.D. degree in automatic control from INPG, Grenoble, France, in 2001. He is currently a Professor of automatic control with the Electronics Engineering Department, TecNM/CENIDET, Cuernavaca, Mexico. His current research focuses on systems identification, model validation, and process control for clean energy systems. His applications deal with PEMFC, storage technology, electric vehicles, hybrid generation systems, and biofuels.

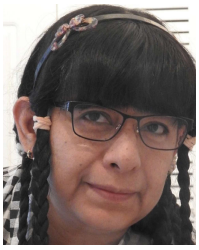

GUADALUPE LOPEZ LOPEZ received the Ph.D. degree in process engineering from the University Aix-Marseille III, France, in 2002. She realized a postdoctoral fellowship at ENSAM, Aix-en-Provence, in 2009. She is currently a Professor of automatic control with the Electronics Engineering Department, TecNM/CENIDET, Cuernavaca, Mexico. Her research includes process modeling, simulation, and control, with a focus on their applications in clean energy. In particular on PEMFC, electric vehicles, energy storage systems, and biofuels.